Emerging Contaminants 9 (2023) 100224

Contents lists available at ScienceDirect

Emerging Contaminants

journal homepage: www.keaipublishing.com/en/journals/emerging-contaminants

Nano-zinc oxide fibers: Synthesis, characterization, adsorption of acid blue 92 dye, isotherms, thermodynamics and kinetics

Deepro Sanjid Qais [a], Md Nazrul Islam [a], Mohd Hafiz Dzarfan Othman [b], H.N.M. Ekramul Mahmud [c], Md Emran Quayum [a], Md Anwarul Islam [a], Iqbal Mohammad Ibrahim Ismail [d], Ahsan Habib [a, *]

[a] Department of Chemistry, Faculty of Science, University of Dhaka, Dhaka, 1000, Bangladesh
[b] Advanced Membrane Technology Research Centre (AMTEC), School of Chemical and Energy Engineering (FCEE), Universiti Teknologi Malaysia, 81310 UTM, Skudai, Johor, Malaysia
[c] Department of Chemistry, Universiti Malaya, Lembah Pantai, 50603, Kuala Lumpur, Malaysia
[d] The Center of Excellence in Environmental Studies and Department of Chemistry, King Abdulaziz University, Jeddah, 21589, Saudi Arabia

ARTICLE INFO

Article history:
Received 6 January 2023
Received in revised form
28 January 2023
Accepted 27 February 2023
Available online 5 March 2023

Keywords:
Nano-ZnO fiber
Polyethylene glycol (PEG)
Azo dye
Adsorption isotherms and kinetics
Water treatment

ABSTRACT

Surface water is significantly contaminated by different dyes and pigments around the world due to rapid industrialization, especially textile/dyeing. Bangladesh's export-driven textile industry has grown dramatically over the past few decades, severely contaminating the nearby waterways. In this study, nano-zinc oxide was synthesized through precipitation method in the presence of PEG 400. SEM, XRD, and FTIR techniques were used to characterize the synthesized ZnO and revealed that it was pure, fiber-like, and essentially wurtzite. Nano-ZnO was used to remove the ionic dye acid blue 92 (AB 92) from aqueous solution in order to test its effectiveness as an adsorbent. The effects of pH, adsorbent dosage, AB 92 concentration, and contact time were investigated in order to optimize the adsorption process. According to correlation coefficients (R^2) and the Redlich-Peterson model's fitting, the adsorption process followed the Freundlich isotherm at higher temperature and the Langmuir isotherm at lower temperature. The adsorption process was found to be endothermic and spontaneous. For adsorption thermodynamics, ΔH was found to be $+20.32$ kJmol^{-1}, and ΔG was varied from -1.86 to -3.84 kJmol^{-1} as the temperature increased from 291 to 317 K. The adsorption kinetics exhibited pseudo second order. The Temkin isotherm and Elovich kinetic models suggested that the process was chemisorption. The nano-ZnO showed tremendous re-usability as an adsorbent for the removal of AB 92. The results are suggesting for designing nano-ZnO-based methods to remove organic pollutants efficiently from industrial effluents for ecological and sustainable development. The mechanism of formation of nano-ZnO fiber and adsorption of anionic dye on nano-ZnO are also explored.
© 2023 The Authors. Publishing services by Elsevier B.V. on behalf of KeAi Communications Co. Ltd. This is an open access article under the CC BY-NC-ND license (http://creativecommons.org/licenses/by-nc-nd/4.0/).

1. Introduction

Bangladesh's GDP is based primarily on its export-oriented textile sector. In 2010, the GDP contribution of export-oriented textile industries was 17.9%; by 2023, this contribution is expected to increase to 25%. On the other hand, because the processes employed by the textile industry utilize a lot of water and various chemicals, they also discharge a lot of contaminated effluents, particularly with synthetic dyes, into the nearby water bodies [1–7]. Even though the Bangladeshi Department of Environment (DoE) has mandated that every textile facility have an effluent treatment plant (ETP), these facilities have not been operating effectively [8]. Waterbodies close to the textile and dyeing industry are consequently highly contaminated [1–5].

Synthetic dyes have been extensively employed in a variety of industries, including textile and dyeing [9], leather, printing, paper, plastics, cosmetics, pharmaceuticals, petrochemicals, and other industries [10,11]. Around the world, synthetic dyes are produced and used in diverse industrial units at a rate of about 700,000

* Corresponding author.
E-mail address: habibchem@du.ac.bd (A. Habib).
Peer review under responsibility of KeAi Communications Co., Ltd.

https://doi.org/10.1016/j.emcon.2023.100224
2405-6650/© 2023 The Authors. Publishing services by Elsevier B.V. on behalf of KeAi Communications Co. Ltd. This is an open access article under the CC BY-NC-ND license (http://creativecommons.org/licenses/by-nc-nd/4.0/).

metric tons annually [12–14]. The textile sector uses 60–70% of these synthetic dyes [15–17]. It is important to note that azo dyes contain aromatic amines (AAs), which are released when they come into contact with skin due to bacterial biotransformation [17–21]. These AAs could cause human mutagenesis and/or cancer [18]. As a result, the European Union (Annex XVII of the REACH regulation; No, 1907/2006) [22] (EC, 2009) and North America have banned the use of many azo dyes that release the hazardous AAs in textiles [23].

The majority of the dyes are released into neighboring water bodies as industrial effluents because only a small portion is used for staining during the dyeing process. Therefore, it is essential to develop an efficient and cost-effective method for removing unstained azo dyes from industrial effluents in order to protect human health and the environment. For the purpose of removing and/or mineralizing organic pollutants from industrial effluents, a variety of methods have already been developed. Among them, adsorption [24–31], oxidation [2–6,32], photocatalytic degradation [1,3,33,34], coagulation-flocculation [35,36], and microbial-based process [37–40] have shown to be the most successful methods. The adsorption method has been widely employed to remove pollutants from aqueous solutions, notably organic dyes because of its many benefits, including cost effectiveness, substantial removal efficiency, and the absence of secondary pollution [13,24–28,41].

In order to remove dyes and metal ions from aqueous solutions, metal oxides and metal nanoparticles have been used as adsorbents, including MgO [13], Fe_3O_4/MgO nanoparticles [42], nano-ZnO [29–31,43,44], Mn-nanoparticles [45], Ni/Fe and Mg/Fe layered double hydroxides [46], nanofibrous metal-organic membranes [47,48] and modified-SiO_2 nanoparticles [49]. It has been found that for the removal of organic dyes, nano-rod ZnO shown greater adsorption effectiveness than spherical ZnO [50]. Therefore, efforts have been made to synthesize nano-ZnO that resembles fibers and has a greater adsorption effectiveness than rod- and/or spherical nano-ZnO.

In this study, nano-ZnO fibers were synthesized by a precipitation process, and they were subsequently examined using scanning electron microscopy (SEM), X-ray diffraction (XRD), and Fourier transform-infrared spectroscopy (FT-IR) methods. The anionic dye acid blue 92 (AB 92) (Scheme 1) was removed from an aqueous solution using the as-prepared nano-ZnO under dark conditions by adjusting the temperature, pH, and concentration of the solution. In addition, efforts have been made to compare the nano-ZnO fibers' ability to adsorb cationic dyes like methylene blue (MB) and rhodamine B (RB) to anionic AB 92 in the dark.

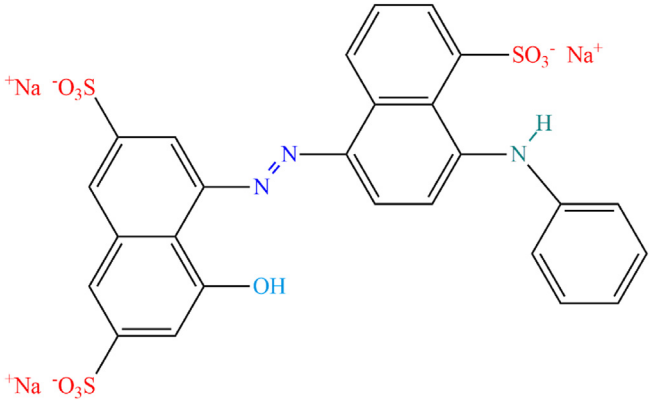

Scheme 1. Structure of acid blue 92 (AB92), trisodium 4-[(4-anilino-5-sulfonaphthalen-1-yl)diazinyl]-5-hydroxynaphthalene-2,7-disulfonate ($C_{26}H_{16}N_3O_{10}S_3Na_3$; M. Mass: 695.58).

2. Experimental

2.1. Materials

Acid blue 92 (AB 92) dye (Scheme 1) was purchased from local dye sellers. The adsorption maximum, λ_{max}, of AB 92 is 570 nm. Hydrochloric acid, sodium chloride, ammonia and polyethylene glycol 400 (PEG 400) solution were purchased from Merck, Darmstadt, Germany. No additional purification was done before using all of the chemicals. Throughout the studies, distilled water was used.

2.2. Synthesis and characterization of nano-ZnO

Ammonia solution was added to zinc nitrate solution together with 1% PEG 400 to precipitate fiber-like nano-zinc oxide. The precipitate ZnO was at least three times rinsed with distilled water before being allowed to air dry. To thoroughly remove water, the air dried ZnO precipitate was put in a desiccator containing silica gel. Scanning electron microscope (SEM: model S–3400 N, Hitachi, Tokyo, Japan), X-ray diffraction (XRD: Bruker DB-Advance X-ray diffractometer, Germany), and Fourier Transform infrared (FTIR: IR-Prestige 21 Shimadzu, Japan) techniques were used to analyze the prepared zinc oxide.

2.3. Preparation of dye solution

A small quantity of AB 92 dye was taken to prepare a concentrated dye solution in a 50 mL volumetric flask. A tiny amount of the stock solution was pipetted into a 100 mL volumetric flask and poured in before being fully topped off with distilled water. Using a UV–Vis spectrophotometer (UV-160A, Shimadzu Corporation, Kyoto, Japan) to record the absorbance at the AB 92 dye's absorption maximum, $\lambda_{max} = 570$ nm, the concentration of the solution was determined. The molar absorptivity calculated from the Beer-Lambert's equation was used to calculate the final dye concentration from the absorbance:

$$A = \varepsilon cl \quad (1)$$

where, A is absorbance, ε is molar absorptivity of AB 92 ($\varepsilon = 17{,}500$ $Lmol^{-1}cm^{-1}$), l is the cell constant (1 cm) and c is the concentration of AB 92.

2.4. Adsorption procedure

In a series of trials, only one parameter-the dye concentration-was altered while the other three-adsorbent dosage, pH, and temperature-remained same. When the solution pH was 7.0 at 298 K, the dye concentration and adsorbent dosage were varied within a range from 25.43 to 67.34 mgL^{-1} at 1.00 gL^{-1} of nano-ZnO and 0.40 to 3.00 gL^{-1} at 45.32 mgL^{-1} of AB 92, respectively. With a dye concentration of 45.32 mgL^{-1} and an adsorbent dosage of 1.00 gL^{-1}, the solution's pH and temperature were also adjusted, ranging from 5.0 to 9.0 at 298 K and 291–317 K at pH 7.0, respectively. This is due to the fact that ZnO dissolves at low solution pH, namely $\leq$4.5. The experiments were all conducted in complete darkness.

2.5. Adsorption efficiency and equilibrium adsorption quantity

Equation (2) was used to quantify adsorption efficiency in percent removal (%), and equation (3) was utilized to get the equilibrium adsorption quantity (q_e).

$$Removal\ (\%) = \frac{c_0 - c_t}{c_0} \times 100 \quad (2)$$

$$Adsorption\ quantity\ (q_e) = \frac{c_0 - c_t}{W} \times V \quad (3)$$

where c_0 and c_t are initial and at time t dye concentration, respectively where q_e is the equilibrium adsorption quantity, V is volume of the experimental solution (100 mL) and W is the amount of ZnO.

2.6. Adsorption isotherms

Equations (4)–(7) were used to fit the experimental data into the Langmuir, Freundlich, Redlich-Peterson, and Temkin adsorption isotherm models in order to optimize the adsorption process [51–54].

$$q_e = \frac{q_m K_L c_e}{1 + K_L c_e} \quad (4)$$

$$q_e = K_F c_e^{\frac{1}{n}} \quad (5)$$

$$q_e = \frac{A\ c_e}{1 + B\ c_e^{g}} \quad (6)$$

$$q_e = \frac{RT}{b_T}\ ln(A_T c_e) \quad (7)$$

where c_e is the equilibrium concentration of AB 92, q_m (mgg^{-1}) is the maximum adsorption capacity of nano-ZnO fiber corresponding to monolayer formation where 'K_L' is a coefficient related to the energy of adsorption in the Langmuir isotherm. The Freundlich isotherm's constants are K_F and n. K_F is the nano-ability ZnO's to adsorb AB 92 across many layers, and n is the adsorption's strength. The Redlich-Peterson isotherm constants, A, B, and g, are used to assess whether the adsorption process follows the Freundlich or Langmuir isotherm. The Temkin constants are A_T (Lmg^{-1}) and b_T ($Jmol^{-1}$). The terms "b_T" and "A_T" refer to the heat of adsorption and the equilibrium binding constant that corresponds to the highest binding energy, respectively. The universal gas constant is R (8.314 J/mol K), while the absolute temperature is 298 K. The non-linear regression plot of q_e vs c_e was used to obtain the values of the adsorption model parameters.

2.7. Adsorption thermodynamics

The effects of temperature on the adsorption process were investigated by studying the adsorption of AB 92 onto the nano-ZnO fiber at various temperatures. Equations (8)–(10) were used to calculate the thermodynamic parameters for the adsorption of AB 92 onto the nano-ZnO fiber, including enthalpy (ΔH), entropy (ΔS), and Gibb's free energy (ΔG) [55].

$$K_d = \frac{q_e}{c_e} \quad (8)$$

$$ln\ K_d = -\frac{\Delta H}{RT} + \frac{\Delta S}{R} \quad (9)$$

where K_d stands for thermodynamic equilibrium constant.

$$\Delta G = \Delta H - T\Delta S \quad (10)$$

2.8. Adsorption kinetics

Pseudo-first order and pseudo-second order kinetic models were utilized to investigate the adsorption mechanism of the AB 92 dye onto the nano-ZnO with a fiber-like structure. To determine whether the adsorption kinetics were pseudo first order (equ. 11) or pseudo second order (equ. 12), the experimental data was fitted into the Lagergren and Ho-Mckay kinetic models. Using the Elovich model, the rate of chemisorption was investigated (equ. 13). The rate equations can be written as follows [53–56]:

$$q_t = q_e\left(1 - e^{-k_1 t}\right) \quad (11)$$

$$q_t = \frac{k_2 {q_e}^2 t}{1 + k_2 q_e t} \quad (12)$$

$$q_t = \frac{1}{B} ln(1 + ABt) \quad (13)$$

where k_1 (min^{-1}) and k_2 ($gmg^{-1}min^{-1}$) are the adsorption rate constants of pseudo-first and pseudo-second order kinetic models, respectively, A and B are the initial rate of chemisorption and desorption for the Elovich kinetic model respectively, and q_t and q_e (both in mgg^{-1}) are the equilibrium adsorption uptake at time = t and t = ∞, respectively.

3. Results and discussion

3.1. Characterization of Nano-ZnO

Fig. 1(a), (b), and (c) show, the SEM image, XRD pattern, and FTIR spectrum of the nano-ZnO as synthesized, respectively. As seen in Fig. 1, the majority of the synthesized nano-ZnO is fiber-like and somewhat aggregated. XRD pattern of the synthesized ZnO is shown in Fig. 1(b). The typical peaks (100), (002), (101), (102), (110), (103), (112), (201), and (202) of pure ZnO are observed in the XRD pattern. The XRD data are in good agreement with the typical values of the wurtzite structure of ZnO (JCPDS: 36–1451) (inset in Fig. 1(b)) [57]. In light of this, it is concluded that the precipitation method utilizing 1% PEG 400 allowed the synthesis of nano-ZnO fibers with a perfect wurtzite structure.

In a previous work, we attempted to synthesize rod-like nano-ZnO in the presence of surfactants such as sodium dodecyl sulfate (SDS), cetyl trimethyl ammonium bromide (CTAB), and triton X-100, and found that SDS could control the formation of rod-like nano-ZnO [57,59]. Anionic SDS molecules are supposed to adsorb on the seed ZnO during nucleation. It is impossible for additional anionic SDS species to adsorb from other sides due to the bulky group of the SDS molecules, but it may be possible for unidirectional rod-like nano-ZnO to develop. Due to the structural differences between PEG and SDS, each surfactant functions differently. PEG 400 was employed in this investigation to regulate the emergence of different nanostructured ZnOs. Nano-ZnO forms fiber-like nano-ZnO in the precipitation method due to PEG molecules. Although the precise mechanism of PEG-assisted nano-ZnO fiber formation is unknown, a hypothetical explanation based on existing knowledge is given below [60–66].

The PEG molecules are essential in the wet chemical process for changing the spherical nanostructures of ZnO particles to wire/rod-

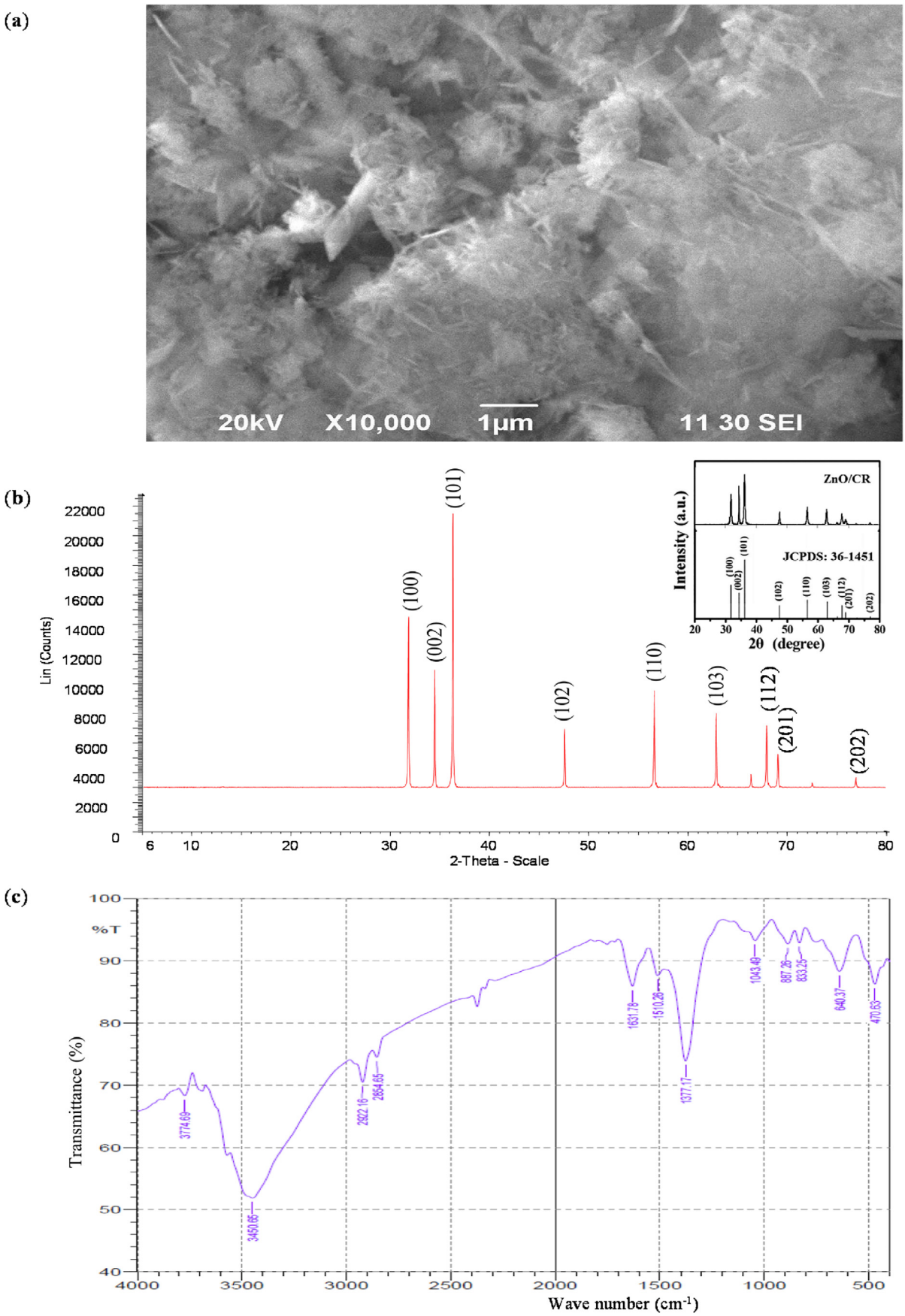

Fig. 1. Characterization of the prepared nano-ZnO (a) SEM image, (b) XRD pattern and (c) FTIR spectrum. Inset is for JCPDS:36–1451 of ZnO [58].

like nanostructures [60,61]. Nonionic surfactants PEG molecules with the formula [$H(OCH_2CH_2)_nOH$] have a hydrophilic ether group (-O-) and a hydrophobic ethylene unit (-CH_2-CH_2-). Due to a strong repelling tendency between water molecules and the hydrophobic ethylene, −CH_2-CH_2-, unit, water molecules are associated with the nonionic ether group, -O- [62]. The PEG molecules therefore self-assembled on the surface, with the hydrophilic end pointing in the direction of the water molecule and the hydrophobic end pointing outward.

Before exploring the mechanism of formation of the nano-ZnO fiber, it is essential to take Zn(II) speciation in the aqueous system into account. On the basis of a speciation diagram, Zn(II) predominantly present (~90%) in aqueous solution as $Zn(II)_{aq}$ ($[Zn(II)(H_2O)_6]^{2+}$) species at pH 6.9 and speciation data reveal the stepwise formation of $[Zn(H_2O)_{6-n}(OH)_n]^{2-n}$ species (*i.e.*, $Zn(OH)^{+}_{aq}$, $Zn(OH)^{0}_{2aq}$, $Zn(OH)^{-}_{3aq}$, $Zn(OH)^{2-}_{4\ aq}$) with solution pH [63,64]. Due to electrostatic forces of attraction between the cationic $Zn(II)_{aq}$ ion and the lone pairs of electrons of the oxygen atom, the cationic $Zn(II)_{aq}$ ion in acidic solution coordinated with the oxygen atom of the ether group, remaining Zn−O as a template unit for the crystal growth. The $Zn(II)_{aq}$ ion tends to coordinate with the ether oxygen atom (-O-) because it is more basic than the oxygen atom in water molecules. This can be explained by the fact that water has a lower proton affinity (PA: 703 kJmol-1) than ether oxygen, which has a higher PA of 828.4 $kJmol^{-1}$ [66].

As was previously mentioned, the formation of different hydroxozinc(II) species is influenced by the pH of the solution. These species can exist in soluble (aqua) or insoluble (colloids) forms depending on their solubility products. Due to hydrogen bonding between the hydroxyl groups of the incoming hydroxozinc(II) species and the Zn−O template, the Zn(II) ion must be present in both the soluble (aqua) and insoluble (colloids) forms [64]. The amount of colloidal ZnO(H) particles that form and deposit on the Zn−O template increases as the pH of the solution rises. Hydrophobic cone type ethylene units facilitate one-dimensional (1D) nano-ZnO crystal formation. Scheme 2 shows a potential mechanism for the growth of nano-ZnO fiber as a 1D crystal. The amount to which colloidal ZnO(H) particles adsorb on the Zn−O template determines the length of the fiber-like ZnO [60−62]. PEG concentration and chain length could lead to structural deformation and fiber-like nano-ZnO. It is feasible to create rod- and/or fiber-like nanostructures of ZnO because it displays polar crystal growth in the [0 0 0 1] direction, as demonstrated in Fig. 1(a) [60−62].

The FT-IR spectra of the prepared ZnO, measured in the 4000-400 cm^{-1} range, is shown in Fig. 1(c). It is depicted that the synthesized ZnO had vibrational peaks at 470, 640, 737, 833, 887, 1043, 1377, 1510, 1631, 2854, 2922, and 3450 cm^{-1} (Fig. 1(c)). While the vibrational peaks appeared in a range from 1700 to 600 cm^{-1} corresponding to C═O, C−O, and C−H vibrations, the peak at 470 cm^{-1} was assigned to the Zn−O stretching band [67]. The peaks that appeared in the range of 2854−3450 cm^{-1} were attributed to the O−H stretching vibrations and the bending modes of adsorbed water molecules, respectively [68]. PEG was used as a capping agent to produce nano-ZnO fiber using the precipitation method. The presence of PEG caused the C═O, C−O, and C−H vibration bands to show up in the IR spectra.

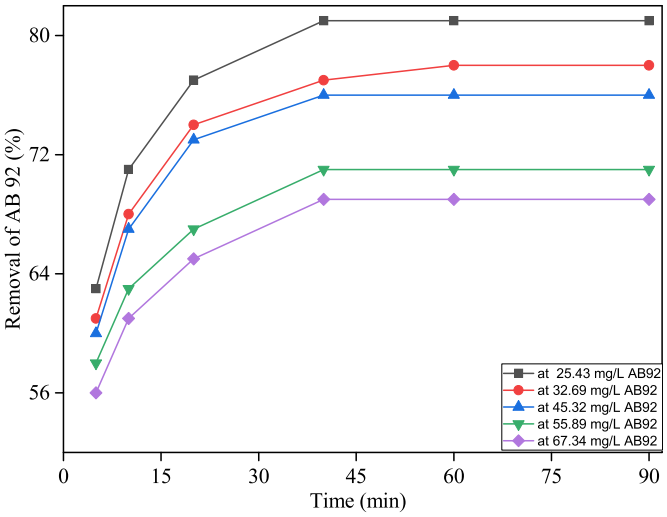

Fig. 2. Effect of initial dye concentration on the removal of AB 92 in the presence of 1 gL^{-1} of nano-ZnO fiber. Solution pH: 7.0; Temperature: 298 K.

3.2. Effect initial dye concentrations on adsorption of AB 92 dye

In order to optimize the adsorbent dose and equilibrium time, it was investigated how initial dye concentrations affected the adsorption of AB 92 onto the nano-ZnO fiber. It makes sense that the surface area that is available for adsorption will be at its peak early on, especially in the first 5 min, leading to a large increase in adsorption efficiency. As the adsorption process progresses, the degree of adsorption decreases with contact time. Because adsorbate molecules occupy the majority of the active sites at the beginning of the adsorption process, the amount of adsorbent is limited over time. The initial adsorbate concentration results in various concentrations of adsorbate molecules on the active sites of adsorbents at a certain amount of the adsorbent [69,70].

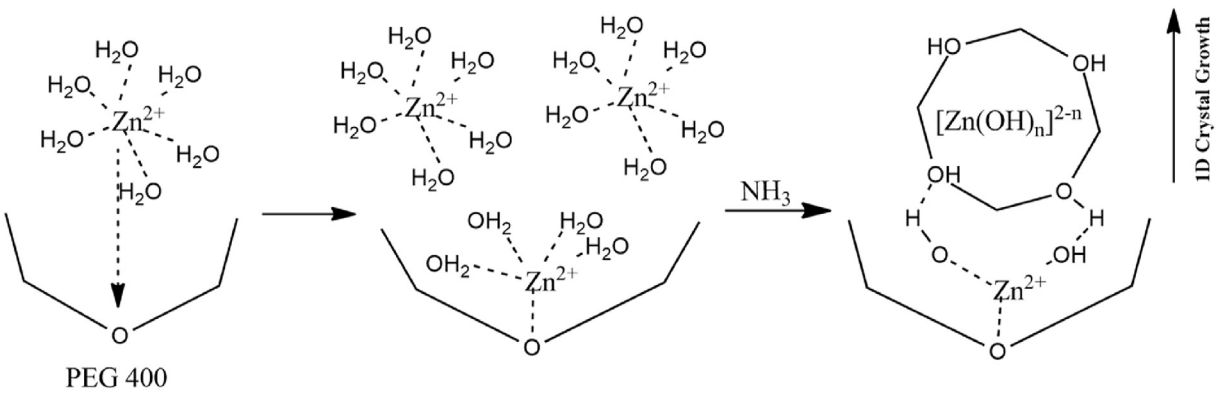

Scheme 2. A proposed mechanism of formation of nano-ZnO fiber by precipitation method in the presence of PEG 400.

The impact of initial AB 92 dye concentrations is depicted in Fig. 2 in the presence of 1.00 gL^{-1} of nano-ZnO at pH 7.0 and 298 K. As seen in Fig. 2, all dye concentrations experienced a rapid increase in adsorption, and equilibrium was reached within 40 min. No discernible adsorption was seen after 40 min. The maximum removal of the AB 92 dye from aqueous solution was seen at the low concentration (25.43 mgL^{-1}), whereas the minimum removal was seen at the highest concentration (67.34 mgL^{-1}). Finding the highest removal of AB 92 at the lowest dye concentration (25.34 mgL^{-1}) in the presence of a constant amount of nano-ZnO seems plausible.

3.3. Effect of adsorbent dose on adsorption of AB 92 dye

The effect of dosage on AB 92 adsorption is shown in Fig. 3. Fig. 3 illustrates how the amount of nano-ZnO enhances the removal effectiveness of the AB 92 dyes. It makes sense that the maximum number of active sites will exist at the greater adsorbent dosage.

The maximum removal of AB 92 for 1.00 gL^{-1} of nano-ZnO fiber was 78%, whereas just 29% was for 0.40 gL^{-1} of nano-ZnO fiber. 98% of AB 92 was removed using larger adsorbent doses, like 3.00 gL^{-1} within 5 min. There was no more removal while the adsorption process progressed. This is due to the fact that an excess of active sites on nano-ZnO surfaces remain empty because a specific number of AB 92 dye molecules were entirely adsorbed into corresponding active sites [12,24].

3.4. Effect of pH on adsorption of AB 92 dye

The removal of the AB 92 dye in the presence of the nano-ZnO fiber in aqueous solution at 298 K as a function of solution pH is shown in Fig. 4. The highest removal (78%) was seen for solution pH 8.0, followed by pH 7.0 (76%), at the equilibrium time (40 min). However, that dropped either the solution pH increased or decreased, as shown in Fig. 4. The presence of anions in the aqueous solution can cause the anionic AB 92 dye molecules to compete with one another for the same adsorption sites, while the positively charged nano-ZnO surface can both bind to and compete with the anionic AB 92 for adsorbent sites. It follows that the presence of other ions will inhibit anionic AB 92 adsorption and reduce its effectiveness. Because of this, 77% of the maximum AB 92 dye

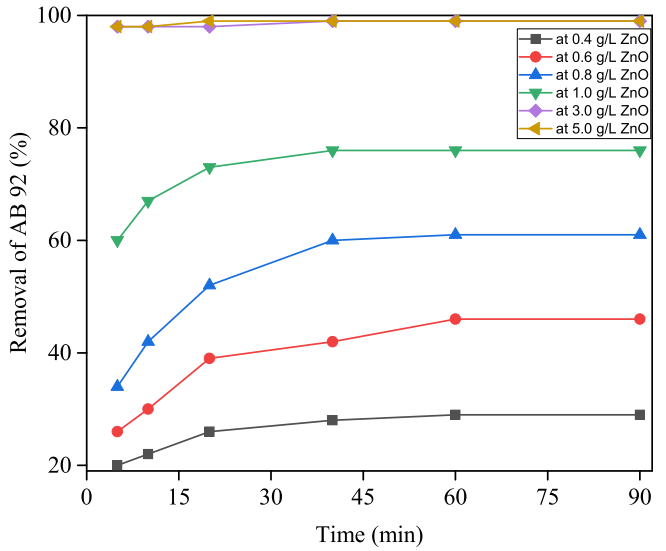

Fig. 3. Effect of adsorbent dose on the removal of AB 92. [AB 92]: 45.32 mgL^{-1}; Solution pH: 7.0; Temperature: 298 K.

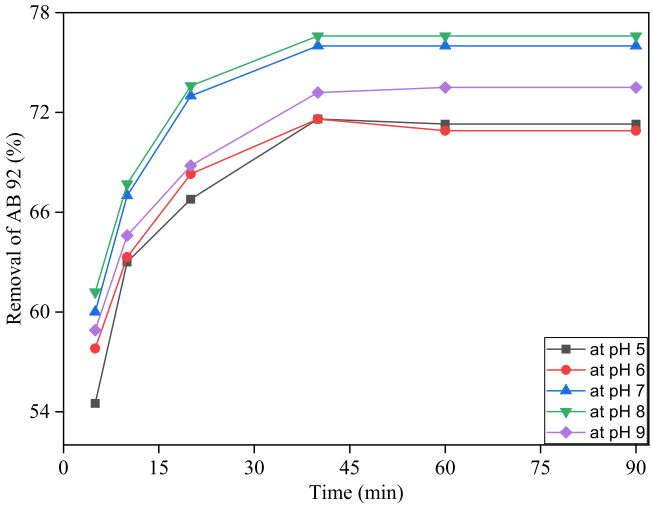

Fig. 4. Effect of pH on the removal of AB 92 in the presence of nano-ZnO fiber (1.00 gL^{-1}). [AB 92]: 45.32 mgL^{-1}; Temperature: 298 K.

adsorption in the presence of nano-ZnO was realized.

The surface of nano-ZnO is positively charged ($Zn(OH)^{+}$) up to a solution pH below 8.9 and then turns negatively charged (ZnO^{-}) as the solution pH rises above 8.9 because the zero-point charge of nano-ZnO is 8.9 [1,71]. The dye molecules in aqueous medium should exist as electrically neutral species throughout the experimental pH range of 5.0–9.0 because the pK_a value of the AB 92 dye is 11.22. However, it is reasonable to expect the sodiated AB 92 dye molecules to be present in the aqueous solution as the partially ionized form, $[AB\ 92]^{-}$, below the pKa value, 11.22, where Na^{+} serves as a counter ion. In the pH range from neutral to alkaline as opposed to acidic pH, the proportion of ionized AB 92 dye molecules will be larger. It is anticipated that when the pH of the solution lowers from neutral to acidic, the AB 92 dye molecules will gain proton (H^{+}) and become positively charged. This is caused by the azo group, (-N=N-), presence in the AB 92 dye molecules. The minimum adsorption (5%) of cationic dyes like methylene blue (MB) and rhodamine B (RB) onto the nano-ZnO (1.00 gL^{-1}) at solution pH 7.0 at 298 K is extremely desirable, as illustrated in Fig. 5. These findings revealed that at pH 8.9 (*zpc* of nano-ZnO), the surface charge of the prepared nano-ZnO was plainly positive and the adsorption of cationic dyes, such as MB and RB, decreased to a

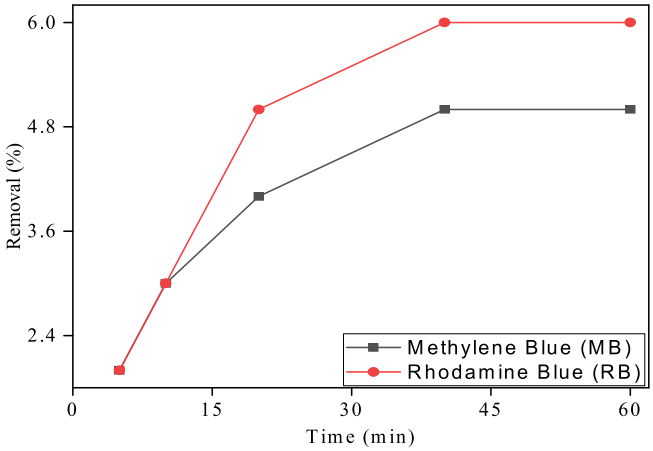

Fig. 5. Removal of methylene blue (MB) and rhodamine B (RB) in the presence of nano-ZnO fiber (1.00 gL^{-1}), [Cationic dye]: 45.55 mgL^{-1}; Temperature: 298 K.

negligible level (5%). The little adsorption of the cation dye molecules onto the positively charged surface of nano-ZnO at pH 8.9 is actually mostly caused by the electrostatic force of repulsion between the two positively charged species.

A significant portion of the AB 92 dye molecules become positively charged at low solution pH (5.0–6.0), which leads to a decreased adsorption efficiency (removal, ~71%) of the cationic dye molecules onto the positively charged surface of nano-ZnO at the equilibrium time, 40 min (Fig. 4). When compared to pH 5–6 at the equilibrium time, the adsorption effectiveness of the AB 92 dye onto the nano-ZnO was slightly higher at pH 9.0 (removal, ~73%). Since the nano-ZnO has a *zpc* of 8.9, it is reasonable to assume that at a pH of 9.0, the majority of its surface-active sites will continue to be positively charged. At a solution pH of 9.0, the majority of the AB 92 dye molecules are anionic, which could marginally increase adsorption efficiency. The experiment was not run at lower pHs like 4.0 or 3.0 since ZnO dissolves at low solution pHs.

3.5. Adsorption isotherms

Adsorption isotherms are mathematical concepts developed through the use of experimental data. The isotherms explain how the adsorbate molecules are distributed throughout the adsorbent surfaces by physisorption and/or chemisorption. The most widely used isotherms, including the Langmuir, Freundlich, and Temkin models, were employed in this study to assess the equilibrium data for AB 92 onto the nano-ZnO fiber in an effort to identify a model that could be applied for the design and optimization of adsorption processes. The Langmuir isotherm is used to describe homogeneous monolayer adsorption [72], the Freundlich isotherm is used to describe heterogeneous multilayer adsorption [73], the Redlich-Peterson isotherm combines the Langmuir and Freundlich isotherms [74], and the Temkin isotherm is used to describe chemisorption [75]. Equations (4)–(7) can be used to express the Langmuir, Freundlich, Redlich-Peterson, and Temkin equations, respectively.

The Langmuir, Freundlich, Redlich-Peterson, and Temkin models are depicted in Fig. 6(a), (b), (c), and (d), respectively. Table 1 contains a summary of the isotherms parameters. These results show that the Langmuir, Freundlich, Redlich-Peterson, and Temkin isotherms almost completely suit the adsorption data because the co-efficient of correlation (R^2) for each isotherm is very close to unity at 291 K. The adsorption data started to depart from the Langmuir model, with $R^2 < 0.95$ at 311K, as the temperature was elevated. The maximal adsorption capacity, q_m, of Langmuir falls dramatically with temperature.

The adsorption process follows the Freundlich isotherm at higher temperatures [7,51,76] whereas the Langmuir isotherm is followed at lower temperatures [44,77–80]. According to the Freundlich model, $1/n = 0$ denotes irreversibility, $1/n < 1$ denotes favorability, while $1/n > 1$ denotes unfavourability [44,80]. As the temperature rose, the 1/n decreased, indicating that the heterogeneous multilayer system was becoming more advantageous.

The Langmuir model will be used if the constant g in the Redlich-Peterson isotherm is one or very close to one; however, the Freundlich model will be used if the constant g deviates from one and Bc_e^g is more than one [51,53,81]. As the temperature rose from 291K to 311K in Fig. 6(c), g changed from 1 to 0.59. B in Table 1 indicates that Bc_e^g is also greater than unity. This proves that the adsorption process followed the Langmuir model at lower temperatures, but that as the temperature rises, the process tends to follow the Freundlich model more closely than the Langmuir model. This suggests that the AB 92 dye molecules deposit homogeneous monolayers onto the nano-ZnO fiber at low temperatures and heterogeneous multilayers at higher temperatures.

As seen in Table 1, A_T and b_T rose with temperature, causing AB 92 molecules to interact with nano-ZnO fiber surfaces more chemically, as predicted by the Temkin model. Since AB 92 is an anionic dye and nano-ZnO has a positive surface charge at pH 7.0, the adsorption process is driven by electrostatic force of attraction [51,53,54]. The maximum adsorption quantity of anionic dye AB 92 is quite high compared to that of cationic dye MB, which only exhibits about 10.70 mgg^{-1} [82] because of the positive surface charge. According to the isotherm data for different temperatures, it can be inferred that at lower temperatures, the adsorption of AB 92 onto the nano-ZnO fiber strongly follows Langmuir, whereas at higher temperatures, the tendency to follow Freundlich and Temkin increases and Langmuir decreases.

3.6. Adsorption thermodynamics

According to Fig. 7, when the solution temperature rises, the AB 92 dye is more effective at adhering to nano-ZnO. In contrast to the adsorption effectiveness of the AB 92 dye on the nano-ZnO at ambient temperature, thermal heating significantly improved it as shown in Fig. 7 [80], but no enhancement was seen at higher temperatures. It should be mentioned that while desorption took place at the maximum temperature, 317 K, equilibrium was reached after 40 min. At the high temperature of 317 K, it is reasonable to see a slight desorption of the deposited AB 92 dye molecules. This is because at the high temperature of 317 K, the nano-ZnO molecules may also absorb thermal energy, leading to a little desorption.

As shown in Fig. 8, the slope and intercept of the plot of $\ln K_d$ vs T^{-1} were used to derive the values of ΔH and ΔS, and ΔG was calculated using equation (9). Table 2 contains a summary of these thermodynamic characteristics. The analysis revealed that ΔH and ΔS had values of +20.32 $kJmol^{-1}$ and +76.21 $Jmol^{-1}K^{-1}$, respectively. These findings demonstrated that chemisorption was the dominant kind of endothermic adsorption.

These findings demonstrated that the adsorption was endothermic in nature and chemisorption was the dominant process [44,83,84]. It is logical to assume that chemisorption is how the AB 92 dye molecules were brought to the nano-ZnO fiber surface. Anionic AB 92 dye species exhibit electrostatic attraction to the nano-ZnO surface, suggesting chemisorption, because the surface charge of nano-ZnO remains positive until solution pH 8.9 (*zpc* of nano-ZnO). Table 2 demonstrates that when temperature rises, the negative values of ΔG for the adsorption process also rise. These results suggested that the spontaneous adsorption of the AB 92 dye onto nano-ZnO.

In terms of thermodynamics, adsorption in the gas phase and that in the solution phase are two quite different processes. The formation of new chemical bonds by adsorbate molecules on the surface of the adsorbent during the gas phase results in the evolution of heat energy, demonstrating the exothermic nature of the process. On the other hand, adsorption in the solution phase is a distinct phenomenon. Depending on the chemical characteristics of both the adsorbent and adsorbate molecules, the adsorbate molecules may be aggregated and/or enclosed in hydration shells. As a result, energy is needed to dissolve the aggregates and/or hydration shells for adsorption. As a result, the system needs a net energy for efficient adsorption, which causes an endothermic process. The adsorption process was determined to be endothermic and spontaneous based on the observed thermodynamic parameters [54,55,85,86].

3.7. Adsorption kinetics

The plot of q_t vs time in Fig. 9 displays the values of the constants for pseudo-first order kinetics, pseudo-second order, and the

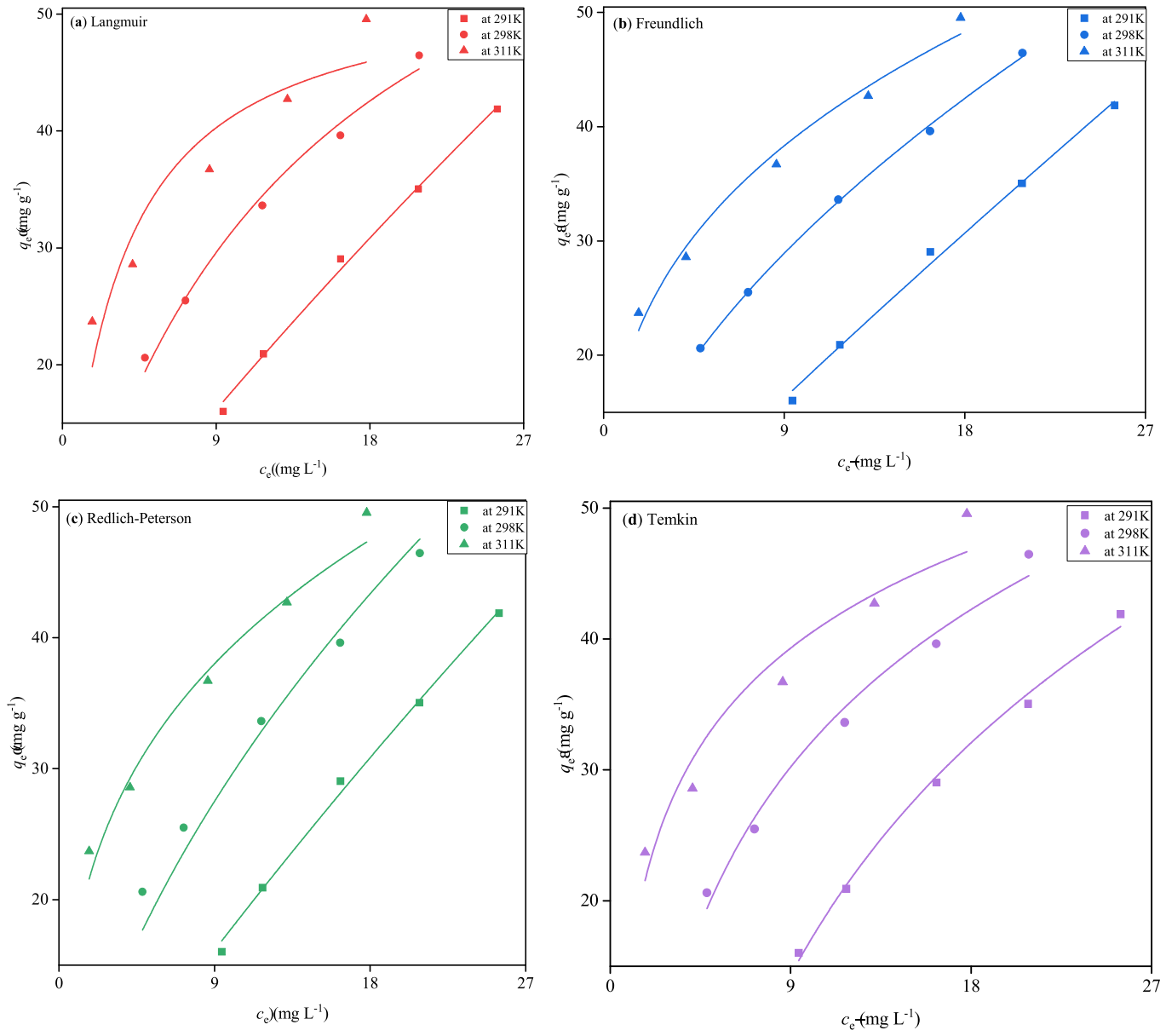

Fig. 6. Adsorption isotherm plots of (a) Langmuir, (b) Freundlich, (c) Redlich-Peterson and (d) Temkin models at different temperatures. Nano-ZnO fiber: 1.00gL^{-1}; Solution pH: 7.0.

Table 1
Isotherm parameters of adsorption of AB 92 onto nano-ZnO fiber at different temperatures. Nano-ZnO: 1.00 g L^{-1}; Solution pH: 7.0.

Temp. (K)	Langmuir			Freundlich			Redlich-Peterson				Temkin		
	q_m (mgg^{-1})	K_L (Lg^{-1})	R^2	K_F (mgg^{-1}((Lmg^{-1})$^{1/n}$)$^{-1}$)	1/n	R^2	A (Lg^{-1})	B (Lmg^{-1})	g	R^2	A_T (Lg-1)	b_T (Jmol^{-1})	R^2
291	343.12	0.005	0.9964	2.15	0.92	0.9953	1.88	0.005	1.00	0.9963	0.19	94.46	0.9952
298	75.72	0.071	0.9894	8.54	0.56	0.9989	6.65	0.326	0.58	0.9652	0.63	142.67	0.9842
311	53.51	0.338	0.8953	18.41	0.33	0.9837	122.05	6.006	0.59	0.9754	4.21	239.25	0.9772

Elovich adsorption kinetics. Table 3 lists each of the parameters. The findings demonstrate that the pseudo first-order reaction's rate constant (k_1) rises as dye concentration (Table 3). The pseudo first order kinetic model did not match the adsorption data satisfactorily since the R^2 values are significantly lower than unity.

Fig. 9(b) presents k_2 and q_e for the adsorption of various concentrations of AB 92 onto the nano-ZnO fiber for pseudo second order adsorption kinetics. Here, as a function of dye concentration, the rate constant, k_2, also drops (Table 3). It should be observed that the values of R^2 were relatively near to one, but they became lower with rising AB 92 concentrations. Both adsorption and chemical kinetics are likely to show such phenomena. The highest number of adsorption sites are initially available, which causes the adsorbate molecules to adhere to the adsorbent surfaces more quickly. The rate of adsorption reduces with time as the number of active sites for a given quantity of adsorbent grows lower. According to the

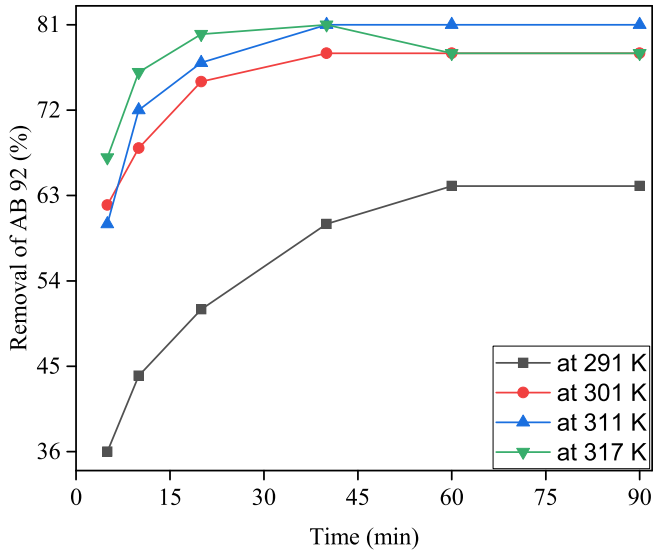

Fig. 7. The effect of temperature on the adsorption efficiency of AB92 dye onto the nano-ZnO fiber surface. [AB92]: 45.32 mgL^{-1}; Nano-ZnO fiber: 1.00 gL^{-1}; Solution pH: 7.0.

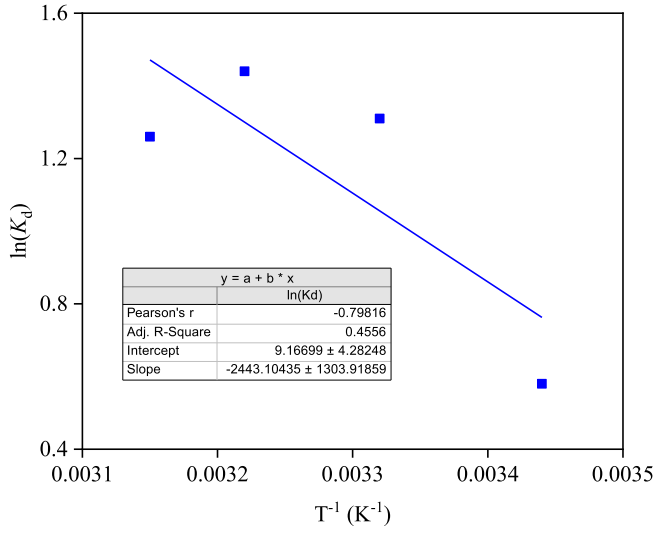

Fig. 8. Plot of logK_d versus 1/T for the calculation of ΔH and ΔS for the adsorption of AB 92 dye onto nano-ZnO fiber surface. [AB 92]: 45.32 mgL^{-1}; Nano-ZnO fiber: 1.00 gL^{-1}; Solution pH: 7.0.

results, pseudo second order kinetics, not pseudo first order kinetics, governs the adsorption of AB 92 onto the nano-ZnO fiber [52,78,87,88].

Fig. 9(c) shows that under the Elovich kinetic model, the R2 values increased as the concentration of AB 92 increased. With increasing AB 92 concentration, the initial adsorption rate, A, likewise increased sharply (Table 3). The electrostatic chemical interaction between the positively charged nano-ZnO surface and the anionic dye increases with higher concentrations of anionic species due to their negative charge, which leads to the conclusion that the adsorption process is dependent on the AB 92 concentration. With increased AB92 concentration, the initial desorption rate, B values decreased even further, indicating a steady adsorption process and a potent interaction between the adsorbent and adsorbate [47,48]. The pseudo second order and Elovich kinetic models of the adsorption process are consistent with the kinetic data, and as the concentration of AB 92 increases, the process tends to favor the Elovich kinetic model over the pseudo second order kinetic model, providing evidence that the process is chemisorption.

3.8. Re-usability of nano-ZnO

In order to look into the stability of the used nano-ZnO as an adsorbent, a dilute solution of NaOH was added to it. More AB 92 removal from the aqueous solution was accomplished using the modified nano-ZnO. At least three or four times as effective as AB 92 could be removed using the produced nano-ZnO.

In the presence of freshly prepared, first re-used, and second re-used nano-ZnO (1.00 gL-1), using 45.32 mgL-1 dye concentration, and at solution pH 7.0 and 298 K, respectively, around 76, 75, and 73% of AB 92 were removed, as shown in Fig. 10. The removal of at least 70% of AB 92 from aqueous solution by nano-ZnO after three or four applications is therefore inferred.

3.9. Mechanism of adsorption and desorption of AB 92 dye

The adsorption of the anionic dye, AB 92, onto the positively charged nano-ZnO surface is mostly dependent on electrostatic force of attraction, as was before mentioned. Prior to a pH of 8.9 in the solution, the surface charge is positive [1]. The stronger anionic species, OH^-, which are more abundant in solutions with pH values above 8.9, induce the adsorbed AB 92 molecules to desorb from the nano-ZnO surface. Scheme 3 illustrates a potential mechanism for this adsorption/desorption process.

3.10. Comparison with other adsorbents

Table 4 lists the maximum adsorbent removal efficiencies of AB 92 from aqueous medium using different adsorbents. As can be seen from Table 4, nano-ZnO fiber was able to remove around 78% of AB 92 from aqueous solution. However, another study showed that single-walled carbon nanotubes (SWCNTs) exhibited remarkable adsorption efficiency for removal of AB 92 from aqueous solution (99.4%). The removal of AB 92 from aqueous solution by the other adsorbents, including Azolla filicoloides, exfoliated graphite, nickel oxide nanoparticle-modified diatomite, and Nd2O3 nanoparticles, was found to be 91%, 96, 95, and 99% efficient. It is quite probable that the presence of anions will cause the dye molecules in AB 92 to compete for adsorption, decreasing the adsorption efficiency. The manufacturer of AB 92 claims that the pKa value of this dye is 11.22 [89], however Balarak et al. (2021) reported that it is only 3.2 [14].

Table 2
The thermodynamic parameters for the adsorption process of AB 92 onto the nano-ZnO fiber. [AB 92]: 45.32 mg L^{-1}; Nano-ZnO fiber: 1.00 g L^{-1}; Solution pH: 7.0.

Temperature (K)	1/T (K^{-1})	ΔG ($kJmol^{-1}$)	ΔH ($kJmol^{-1}$)	ΔS ($Jmol^{-1}$ K^{-1})	R (J mol^{-1} K^{-1})
291	0.00344	−1.89	20.32	76.23	8.316
301	0.00332	−2.66			
311	0.00322	−3.42			
317	0.00315	−3.88			

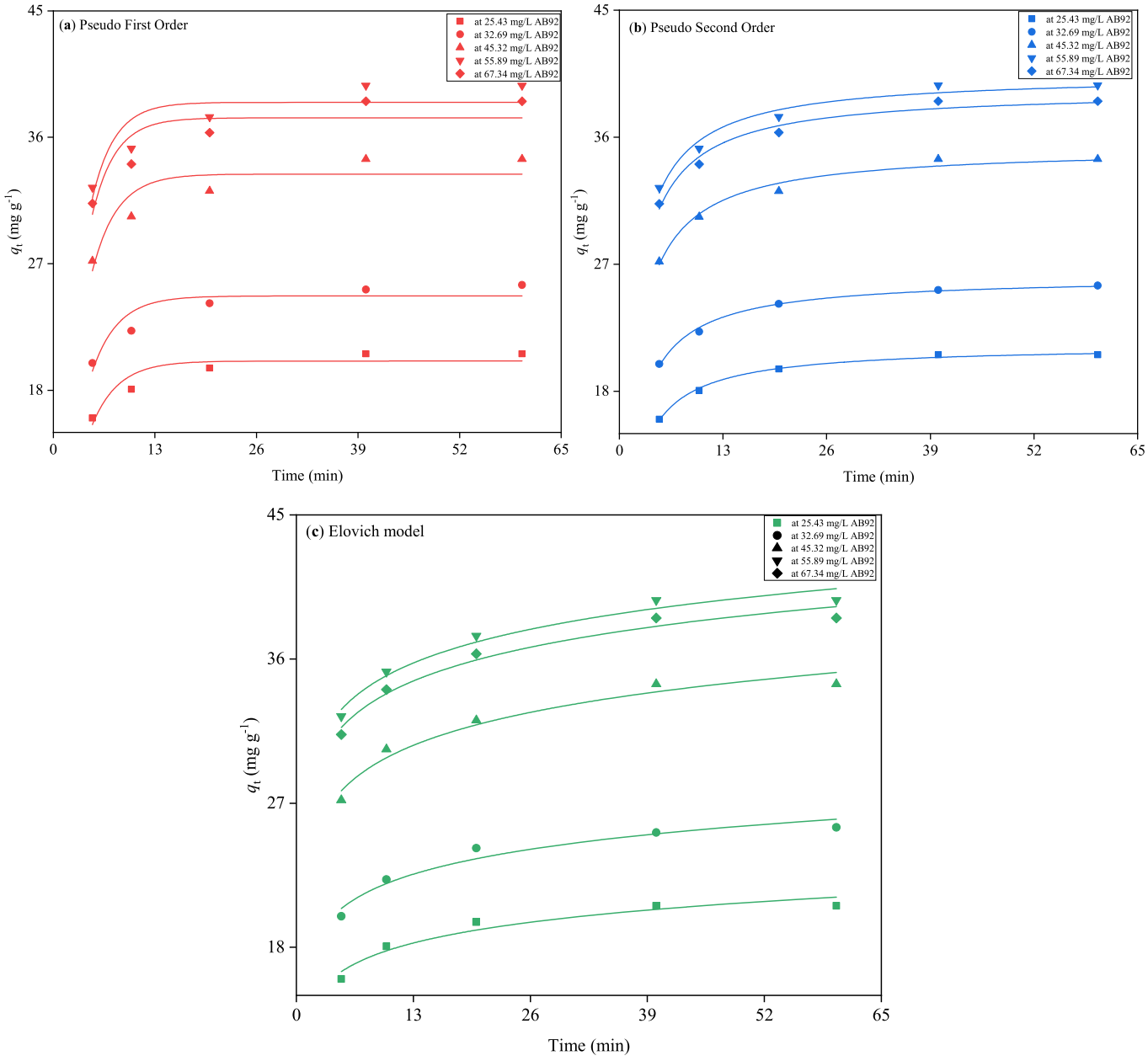

Fig. 9. Adsorption kinetics of different concentrations of AB 92 on nano-ZnO fiber of (a) pseudo first-order, (b) pseudo second-order kinetics and (c) Elovich model. Nano-ZnO fiber: 1.00 gL^{-1}; Solution pH: 7.0; Temperature: 298 K.

Table 3
Kinetic parameters of the adsorption of AB 92 dye onto the nano-ZnO fiber. Nano-ZnO fiber: 1.00 g L^{-1}; Solution pH: 7.0; Temperature: 298 K.

Dye conc. (mgL^{-1})	Pseudo first-order kinetics			Pseudo second-order kinetics			Elovich model		
	k_1 (min^{-1})	q_e (mgg^{-1})	R^2	k_2 (gmg^{-1}min^{-1})	q_e (mgg^{-1})	R^2	A nb(mgg^{-1}min^{-1})	B (mgg^{-1} min^{-1})	R^2
25.43	0.298	20.08	0.8721	0.0282	21.25	0.9950	2500.20	0.534	0.9414
32.69	0.306	24.70	0.8546	0.0239	26.11	0.9948	4057.01	0.446	0.9537
45.32	0.316	33.38	0.8237	0.0184	35.27	0.9827	6845.25	0.337	0.9611
55.89	0.346	38.49	0.7754	0.0183	40.43	0.9748	20886.38	0.329	0.9694
67.34	0.369	41.39	0.7803	0.0182	47.85	0.9755	30583.25	0.329	0.9695

4. Conclusions

Due to the rapid expansion of Bangladesh's textile export-focused industries, untreated effluent pollution of adjacent water sources is a significant problem. The desorption method is one of the wastewater depollution strategies that have already been developed and put into practice. As an adsorbent to remove dyes from aqueous solution, nano-ZnO was synthesized through

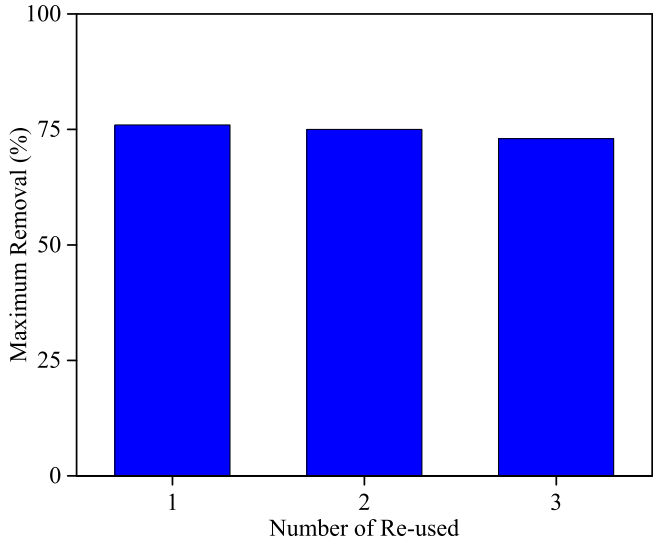

Fig. 10. Adsorption of AB 92 in the presence of freshly prepared and re-used nano-ZnO fiber (1.00 gL^{-1}) for 45.32 mgL^{-1} of dye concentration at pH 7.0 and 298 K.

precipitation. When the nano-ZnO was characterized using SEM, XRD, and FTIR methods, a wurtzite structure and fiber-like appearance were observed. In order to test the effectiveness of the nano-ZnO in its as-prepared form, it was used to remove the model dye AB 92 from aqueous solution. In order to optimize the experimental conditions, the adsorption investigation was conducted with variations in dye concentration, solution pH, adsorbent dosage, and temperature. The maximal removal of AB 92 was determined to be 78% for 45.32 mgL^{-1} of AB 92, pH 7.0, and 1.00 gL^{-1} of adsorbent at 311 K. The adsorption analyses showed that AB 92 adhered to nano-ZnO in a manner that closely matched both the Freundlich and Temkin models. Thermodynamic investigations show that the adsorption process appears to be endothermic and spontaneous. The results of the kinetics experiments showed that the adsorption process closely followed pseudo-second order kinetics. The fiber-like nano-ZnO had a high surface area with a positive surface charge (pH $\leq$ 8.9), and shown improved adsorption and good recyclability for the removal of the anionic AB 92 dye, but only 5% removal for the cationic dyes, MB and RB. The prepared nano-ZnO fiber can therefore be utilized to remove anionic dyes from aqueous industrial effluents and may work well as an adsorbent in practical applications.

Credit authorship contribution statement

Deepro Sanjid Qais: Conceptualization, Methodology, Investigation, Writing – original draft. **Md Nazrul Islam**: Conceptualization, Methodology, Investigation. **Mohd. Hafiz Dzarfan Othman**: Formal analysis, Writing – review & editing. **H.N.M. Ekramul Mahmud**: Formal analysis, Writing – review & editing. **Md. Emran Quayum**: Formal analysis, Fund acquisition. **Md. Anwarul Islam**: Conceptualization, Supervision. **Iqbal Mohammad Ibrahim Ismail**: Writing – review & editing. **Ahsan Habib**: Conceptualization, Methodology, Investigation, Writing – original draft, Writing – review & editing, Fund acquisition, Supervision.

Declaration of competing interest

There are no conflicts of interest declared by the authors.

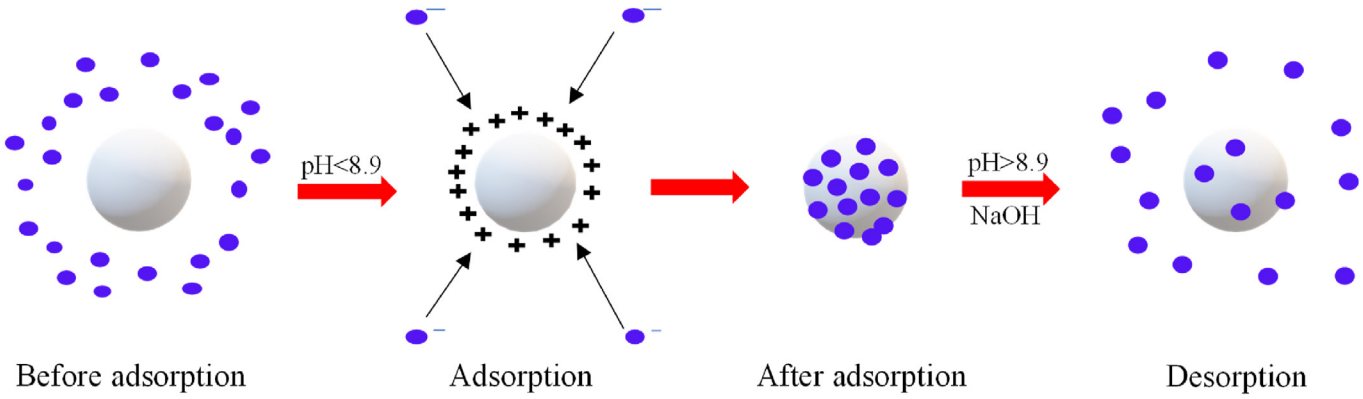

Scheme 3. Proposed mechanism of adsorption and desorption of AB92 in the presence of nano-ZnO fiber.

Table 4
Comparison of nano-ZnO fiber with other adsorbents for AB 92 removal.

Adsorbent	Max removal	Conditions	Reference
Nano-ZnO fiber	78%	[AB 92]: 45.32 mg/L; pH: 7.0; dosage: 1.00 g/L; contact time: 40 min; temperature: 38 °C	This study
SWCNTs	99.4%	[AB 92]: 10 mg/L; pH: 3; dosage: 0.12 g/L; contact time: 75 min; temperature: (30 ± 20C); agitation speed: 180 rpm	Balarak et al. (2021) [14]
Azolla filicoloides	99%	[AB 92]: 10 mg/L; dosage: 7 g/L; pH: 3; contact time: 90 min	Balarak et al. (2016) [90]
Exfoliated graphite	96% (5.02 (gdye/gEG)	[AB 92]: 30 mg/L; feed flow rate: 9.6 mL/min; temperature = 27 ± 2 °C	Goshadrou and Moheb (2011) [91]
Nickel oxide nano- particles-modified diatomite	95%	[AB 92]: 50 mg/L; dosage: 0.1 g/L; pH: 2; temperature: 25 ± 1 °C; speed: 200 rpm; contact time: 90 min	Khalighi Sheshdeh et al. (2012) [92]
Nd_2O_3 nanoparticles	91% (7.3 mg/g)	[AB 92]: 138.5 mg/L; dosage: 0.83 g/L; pH: 3.15; contact time: 50 min; speed: 180 rpm	Ahmadi et al. (2020) [7]

Acknowledgement

Authors are gratefully appreciated by the University of Dhaka, Bangladesh for financial support on the occasion of its 100th anniversary (Development of visible light driven nanoparticles as versatile photocatalysts: an approach to fabricate reusable self-cleaning face masks against COVID-19).

References

[1] A. Habib, I.M.I. Ismail, A.J. Mahmood, M. Rafiqueullah, Photocatalytic decolorization of brilliant golden yellow over TiO_2 and ZnO suspensions, J. Saudi Chem. Soc. 16 (2012) 423–429, https://doi.org/10.1016/j.jscs.2011.02.013.

[2] A. Habib, I.M.I. Ismail, A.J. Mahmood, M. Rafiqueullah, Decolorization and mineralization of brilliant golden yellow (BGY) by fenton and photo-fenton processes, Afr. J. Pure Appl. Chem. 6 (2012) 153–158, https://doi.org/10.5897/AJPAC10.024.

[3] M. Muslim, A. Habib, A.J. Mahmood, T.S.A. Islam, I.M.I. Ismail, Zinc oxide-mediated photocatalytic decolorization of Ponceau S in aqueous suspension by visible light, Int. Nano Lett. 2 (30) (2012), https://doi.org/10.1186/2228-5326-2-30.

[4] M. Muslim, A. Habib, T.S.A. Islam, I.M.I. Ismail, A.J. Mahmood, Decolorization of diazo dye ponceau S by fenton process, Pak. J. Anal. Environ. Chem. 14 (2013) 44–50. http://www.pjaec.pk/index.php/pjaec/article/view/219.

[5] A. Hossain, A.B.M.S. Rayhan, M.J. Raihan, A. Nargis, I.M.I. Ismail, A. Habib, A.J. Mahmood, Kinetics of degradation of Eosin Y by one of the advanced oxidation processes (AOPs)-Fenton's process, Am. J. Anal. Chem. 7 (2016) 863–879, https://doi.org/10.4236/ajac.2016.712074.

[6] N. Ertugay, F.N. Acar, Removal of COD and color from Direct Blue 71 azo dye wastewater by Fenton's oxidation: kinetic study, Arab. J. Chem. 10 (2017) S1158–S1163, https://doi.org/10.1016/j.arabjc.2013.02.009.

[7] S. Ahmadi, L. Mohammadi, A. Rahdar, S. Rahdar, R. Dehghani, C.A. Igwegbe, G.Z. Kyzas, Acid dye removal from aqueous solution by using neodymium(III) oxide nanoadsorbents, Nanomaterials 10 (2020) 556, https://doi.org/10.3390/nano10030556.

[8] Department of Environment (DoE), Guide for Assessment of Effluent Treatment Plants, Department of Environment, Ministry of Environment and Forest, Bangladesh, 2008.

[9] A.F. Doulati, K.H. Badii, L.N. Yousef, S.Z. Shafaei, A.R. Mirhabibi, Adsorption of Direct Red 80 dye from aqueous solution onto almond shells: effect of pH, initial concentration and shell type, J. Hazard Mater. 151 (2008) 730–737, https://doi.org/10.1016/j.jhazmat.2007.06.048.

[10] S. Benkhaya, A. El Harfi, Classifications, properties and applications of textile dyes: a review Appl, J. Environ. Eng. Sci. 3 (2017) 311–320, https://doi.org/10.48422/IMIST.PRSM/ajees-v3i3.9681.

[11] S. Benkhaya, S. M'rabet, A. El Harfi, Classifications, properties, recent synthesis and applications of azo dyes, Heliyon 6 (2020), e03271, https://doi.org/10.1016/j.heliyon.2020.e03271.

[12] N. Hoda, E. Bayram, E. Ayranci, Kinetic and equilibrium studies on the removal of acid dyes from aqueous solutions by adsorption onto activated carbon cloth, J. Hazard Mater. 137 (2006) 344–351, https://doi.org/10.1016/j.jhazmat.2006.02.009.

[13] G.R. Moussavi, M. Mahmoudi, Removal of azo and anthraquinone reactive dyes from industrial wastewaters using MgO nanoparticles, J. Hazard Mater. 168 (2009) 806–812, https://doi.org/10.1016/j.jhazmat.2009.02.097.

[14] D. Balarak, M. Zafariyan, C.A. Igwegbe, K.K. Onyechi, J.O. Ighalo, Adsorption of acid blue 92 dye from aqueous solutions by single-walled carbon nanotubes: isothermal, kinetic, and thermodynamic studies, Environ. Process. 8 (2021) 869–888, https://doi.org/10.1007/s40710-021-00505-3.

[15] K. Lacasse, W. Baumann, Textile Chemicals: Environmental Data and Facts, Springer Berlin, 2004, ISBN 3-540-40815-0.

[16] D. Rawat, V. Mishra, R.S. Sharma, Detoxification of azo dyes in the context of environmental processes, Chemosphere 155 (2016) 591–605, https://doi.org/10.1016/j.chemosphere.2016.04.068.

[17] B.J. Brüschweiler, C. Merlot, Azo dyes in clothing textiles can be cleaved into a series of mutagenic aromatic amines which are not regulated yet, Regul. Toxicol. Pharmacol. 88 (2017) 214–226, https://doi.org/10.1016/j.yrtph.2017.06.012.

[18] T. Platzek, C. Lang, G. Grohmann, U.-S. Gi, W. Baltes, Formation of a carcinogenic aromatic amine from an azo dye by human skin bacteria in vitro, Hum. Exp. Toxicol. 18 (1999) 552–559, https://doi.org/10.1191/096032799678845061.

[19] H.S. Freeman, Aromatic amines: use in azo dye chemistry, Front. Biosci. Landmark 18 (2013) 145–164, https://doi.org/10.2741/4093.

[20] M.F. Akhtar, M. Ashraf, A. Javeed, A. Anjum, S. Ali, A. Sharif, B. Akhtar, A. Khan, I. Altaf, Toxicity appraisal of untreated dyeing industry wastewater based on chemical characterization and short term bioassays, Bull. Environ. Contam. Toxicol. 96 (2016) 502–507, https://doi.org/10.1007/s00128-016-1759-x.

[21] S. Amin, R.P. Rastogi, M.G. Chaubey, K. Jain, J. Divecha, C. Desai, D. Madamwar, Degradation and toxicity analysis of a reactive textile diazo dye-direct red 81 by newly isolated Bacillus sp. DMS2, Front. Microbiol. 11 (2020), 576680, https://doi.org/10.3389/fmicb.2020.576680.

[22] EC Commission Regulation (EC) No 552/2009 of 22 June 2009 Amending Regulation (EC) No 1907/2006 of the European Parliament and of the Council on the Registration, Evaluation, Authorisation and Restriction of Chemicals (REACH) as Regards Annex XVII. http://eur-lex.europa.eu/LexUriServ/LexUriServ.do?uri¼OJ:L:2009:164:0007:0031:EN:PDF.

[23] C. Mo, Azo dye regulations in the United States: an overview. https://www.compliancegate.com/azo-dye-regulations-united-states/#comments, 2020.

[24] A. Habib, Z. Hasan, S. Rahman, A.M.S. Alam, Tuberose sticks as an adsorbent in the removal of methylene blue from aqueous solution, Pak. J. Anal. Environ. Chem. 7 (2006) 112–115. https://inis.iaea.org/search/searchsinglerecord.aspx?recordsFor=SingleRecord&RN=39003567.

[25] R. Han, D. Ding, Y. Xu, W. Zou, Y. Wang, Y. Li, L. Zou, Use of rice husk for the adsorption of Congo red from aqueous solution in column mode, Bioresour. Technol. 99 (2008) 2938–2946, https://doi.org/10.1016/j.biortech.2007.06.027.

[26] P.F.R. Ortega, J.P.C. Trigueiro, M.R. Santos, Â.M.L. Denadai, L.C.A. Oliveira, A.P.C. Teixeira, G.G. Silva, R.L. Lavall, Thermodynamic study of methylene blue adsorption on carbon nanotubes using isothermal titration calorimetry: a simple and rigorous approach, J. Chem. Eng. Data 62 (2017) 729–737, https://doi.org/10.1021/acs.jced.6b00804.

[27] S. Ahmadi, C.A. Igwegbe, Removal of methylene blue on zinc oxide nanoparticles: nonlinear and linear adsorption isotherms and kinetics study, Sigma J. Eng. Nat. Sci. 38 (2020) 289–303. http://eprints.zbmu.ac.ir/id/eprint/3495.

[28] C.A. Igwegbe, O.D. Onukwuli, J.O. Ighalo, P.U. Okoye, Adsorption of cationic dyes on dacryodes edulis seeds activated carbon modifed using phosphoric acid and sodium chloride, Environ. Process 7 (2020) 1151–1171, https://doi.org/10.1007/s40710-020-00467-y.

[29] W.S. Al-Arjan, Zinc oxide nanoparticles and their application in adsorption of toxic dye from aqueous solution, Polymers 14 (2022) 3086, https://doi.org/10.3390/polym14153086.

[30] L.M. Alshandoudi, S.R. Alkindi, T.Y. Alhatmi, A.F. Hassan, Synthesis and characterization of nano zinc oxide/zinc chloride–activated carbon composite based on date palm fronds: adsorption of methylene blue, Biomass Conv. Bioref. (2023), https://doi.org/10.1007/s13399-023-03815-8.

[31] J. Chigova, S. Mudono, Adsorption of chromium (VI) using nano-ZnO doped scrap tire-derived activated carbon, J. Geosci. Environ. Protect. 10 (2022) 121–135, https://doi.org/10.4236/gep.2022.109008.

[32] S. Ahmadi, L. Mohammadi, C.A. Igwegbe, S. Rahdar, A.M. Banach, Application of response surface methodology in the degradation of reactive blue 19 using H_2O_2/MgO nanoparticles advanced oxidation process, Int. J. Ind. Chem. 9 (2018) 241–253, https://doi.org/10.1007/s40090-018-0153-4.

[33] R. Saravanan, S. Karthikeyan, V.K. Gupta, G. Sekaran, V. Narayanan, A. Stephen, Enhanced photocatalytic activity of ZnO/CuO nano-composite for the degradation of textile dye on visible light illumination, Mater. Sci. Eng. C 33 (2013) 91–98, https://doi.org/10.1016/j.msec.2012.08.011.

[34] R. Saravanan, V.K. Gupta, V. Narayanan, A. Stephen, Visible light degradation of textile effluent using novel catalyst ZnO/γ-Mn_2O_3, J. Taiwan Inst. Chem. Eng. 45 (2014) 1910–1917, https://doi.org/10.1016/j.jtice.2013.12.021.

[35] P. Somasundaran, V. Runkana, Investigation of the flocculation of colloidal suspensions by controlling adsorbed layer microstructure and population balance modeling, Chem. Eng. Res. Des. 83 (2005) 905–914, https://doi.org/10.1205/cherd.04345.

[36] I.A. Obiora-Okafo, O.D. Onukwuli, Characterization and optimization of spectrophotometric colour removal from dye containing wastewater by coagulation-focculation, Pol. J. Chem. Technol. 20 (2018) 49–59, https://doi.org/10.2478/pjct-2018-0054.

[37] L. Tan, S. Ning, X. Zhang, S. Shi, Aerobic decolorization and degradation of azo dyes by growing cells of a newly isolated yeast Candida tropicalis TL-F1, Bioresour. Technol. 138 (2013) 307–313, https://doi.org/10.1016/j.biortech.2013.03.183.

[38] S. Agrawal, D. Tipre, B. Patel, S. Dave, Optimization of triazo Acid Black 210 dye degradation by Providencia sp. SRS82 and elucidation of degradation pathway, Process Biochem. 49 (2014) 110–119, https://doi.org/10.1016/j.procbio.2013.10.006.

[39] S.P. Govindwar, M.B. Kurade, D.P. Tamboli, A.N. Kabra, P.J. Kim, T.R. Waghmode, Decolorization and degradation of xenobiotic azo dye reactive yellow-84A and textile effluent by Galactomyces geotrichum, Chemosphere 109 (2014) 234–238, https://doi.org/10.1016/j.chemosphere.2014.02.009.

[40] L. Tan, M. He, L. Song, X. Fu, S. Shi, Aerobic decolorization, degradation and detoxification of azo dyes by a newly isolated salt-tolerant yeast Scheffersomyces spartinae TLHS-SF1, Bioresour. Technol. 203 (2016) 287–294, https://doi.org/10.1016/j.biortech.2015.12.058.

[41] H. Gao, S. Zhao, X. Cheng, X. Wang, L. Zheng, Removal of anionic azo dyes from aqueous solution using magnetic polymer multi-wall carbon nanotube nanocomposite as adsorbent, Chem. Eng. J. 223 (2013) 84–90, https://doi.org/10.1016/j.cej.2013.03.004.

[42] A.N.M. Salem, M.A. Ahmed, M.F. El-Shahat, Selective adsorption of amaranth dye on Fe3O4/MgO nanoparticles, J. Mol. Liq. 219 (2016) 780–788, https://doi.org/10.1016/j.molliq.2016.03.084.

[43] C. Lei, M. Pi, C. Jiang, B. Cheng, J. Yu, Synthesis of hierarchical porous zinc oxide (ZnO) microspheres with highly efficient adsorption of Congo red, J. Colloid Interface Sci. 490 (2017) 242–251, https://doi.org/10.1016/j.jcis.2016.11.049.

[44] M.N. Zafar, Q. Dar, F. Nawaz, M.N. Zafar, M. Iqbal, M.F. Nazar, Effective adsorptive removal of azo dyes over spherical ZnO nanoparticles, J. Mater. Res.

Technol. 8 (2019) 713–725, https://doi.org/10.1016/j.jmrt.2018.06.002.
[45] M. Arshadi, F. Salimi Vahid, J.W.L. Salvacion, M. Soleymanzadeh, Adsorption studies of methyl orange on an immobilized Mn-nanoparticle: kinetic and thermodynamic, RSC Adv. 4 (2014) 16005–16017, https://doi.org/10.1039/C3RA47756H.
[46] R. Elmoubarki, F.Z. Mahjoubi, A. Elhalil, H. Tounsadi, M. Abdennouri, M. Sadiq, S. Qourzal, A. Zouhri, N. Barka, Ni/Fe and Mg/Fe layered double hydroxides and their calcined derivatives: preparation, characterization and application on textile dyes removal, J. Mater. Res. Technol. 6 (2017) 271–283, https://doi.org/10.1016/j.jmrt.2016.09.007.
[47] J.E. Efome, D. Rana T. Matsuura, C.Q. Lan, Insight studies on metal-organic framework nanofibrous membrane adsorption and activation for heavy metal ions removal from aqueous solution, ACS Appl. Mater. Interfaces 10 (2018) 18619–18629, https://doi.org/10.1021/acsami.8b01454.
[48] J.E. Efome, D. Rana, T. Matsuura, C.Q. Lan, Metal–organic frameworks supported on nanofibers to remove heavy metals, J. Mater. Chem.A 6 (2018) 4550–4555, https://doi.org/10.1039/C7TA10428F.
[49] A.S. Patra, S. Ghorai, S. Ghosh, B. Mandal, S. Pal, Selective removal of toxic anionic dyes using a novel nanocomposite derived from cationically modified guar gum and silica nanoparticles, J. Hazard Mater. 301 (2016) 127–136, https://doi.org/10.1016/j.jhazmat.2015.08.042.
[50] P.M. da Silva, M.M. Serna, E. Galego, R.N. Faria Jr., The influence of the nanostructures on the dye adsorption in dye sensitized solar cell, Res. Dev. Material Sci. 15 (2021), 000859, https://doi.org/10.31031/RDMS.2021.15.000859.
[51] M. Belhachemi, F. Addoun, Comparative adsorption isotherms and modeling of methylene blue onto activated carbons, Appl. Water Sci. 1 (2011) 111–117, https://doi.org/10.1007/s13201-011-0014-1.
[52] S. Nethaji, A. Sivasamy, A.B. Mandal, Adsorption isotherms, kinetics and mechanism for the adsorption of cationic and anionic dyes onto carbonaceous particles prepared from Juglans regia shell biomass, Int. J. Environ. Sci. Technol. 10 (2013) 231–242, https://doi.org/10.1007/s13762-012-0112-0.
[53] C.S. Ngakou, G.S. Anagho, H.M. Ngomo, Non-linear regression analysis for the adsorption kinetics and equilibrium isotherm of phenacetin onto activated carbons, Cur. J. App. Sci. Tech. 36 (2019) 1–18, https://doi.org/10.9734/cjast/2019/v36i430246.
[54] H. Zhang, D. Wu, Q. Huang, Z. Liu, X. Luo, S. Xiong, T. Yin, Adsorption kinetics and thermodynamics of yeast β-glucan for off-odor compounds in silver carp mince, Food Chem. 319 (2020), 126232, https://doi.org/10.1016/j.foodchem.2020.126232.
[55] J. Wu, A. Xia, C. Chen, L. Feng, X. Su, X. Wang, Adsorption thermodynamics and dynamics of three typical dyes onto bio-adsorbent spent substrate of Pleurotus eryngii, Int. J. Environ. Res. Publ. Health 16 (2019) 679, https://doi.org/10.3390/ijerph16050679.
[56] J. López-Luna, J.E. Ramírez-Montes, S. Martinez-Vargas, A.I. Martínez, O.F. Mijangos-Ricardez, M.C.A. González-Chávez, R. Carrillo-González, F.A. Solís-Domínguez, C. Cuevas-Díaz, V. Vázquez-Hipólito, Linear and nonlinear kinetic and isotherm adsorption models for arsenic removal by manganese ferrite nanoparticles, SN Appl. Sci. 1 (2019) 950, https://doi.org/10.1007/s42452-019-0977-3.
[57] D. Leila, L.G. Mar, B. Fatima, N. Abddelyamine, B. Ali, H. Nacereddine, Effect of polyethylene glycol and propyltrimethoxysilane on structural and optical properties of zinc oxide nanoparticles synthesized by sol–gel process, J. Theo. Appl. Phy. 12 (2018) 159–167, https://doi.org/10.1007/s40094-018-0303-2.
[58] T.M. Elmorsi, M.H. Elsayed, M.F. Bakr, Enhancing the removal of methylene blue by modified ZnO nanoparticles: kinetics and equilibrium studies, Can. J. Chem. 95 (2017) 590–600, https://doi.org/10.1139/cjc-2016-0456.
[59] M.S. Mahmud, M.J. Raihan, M.N. Islam, D.S. Qais, N. Asim, W.A.W. A Bakar, M.E. Quayum, M.A. Islam, I.M.I. Ismail, A. Habib, Synthesis of solar light driven nanorod-zinc oxide for degradation of rhodamine B, industrial effluent and contaminated river water, Arab. J. Chem. 15 (2022), 104144, https://doi.org/10.1016/j.arabjc.2022.104144.
[60] M.R. Parra, F.Z. Haque, Poly (Ethylene Glycol) (PEG)-assisted shape-controlled synthesis of one-dimensional ZnO nanorods, Optik 126 (2015) 1562–1566, https://doi.org/10.1016/j.ijleo.2015.05.011.
[61] K. Pavani, A. Kumar, ZnO nanostructures: simple routes of synthesis, Int. J. Eng. Res. Technol. 4 (2015) 505–508, https://doi.org/10.17577/IJERTV4IS090518.
[62] M.A. Tshabalala, B.F. Dejene, H.C. Swart, Synthesis and characterization of ZnO nanoparticles using polyethylene glycol (PEG), Physica B Cond. Matter 407 (2012) 1668–1671, https://doi.org/10.1016/j.physb.2011.09.113.
[63] A. Nargis, A. Habib, H.-O.- Rashid, H.B. Harun, M.S.I. Sarker, R. Jin, G. Liu, W. Liu, A.N.M. Al-Razee, K. Chen, M. Cai, Status of multielement in water of the river Buriganga, Bangladesh: aquatic chemistry of metal ions in polluted river water, Emerg. Contam. 7 (2021) 99–115, https://doi.org/10.1016/j.emcon.2021.03.001.
[64] A. Habib, R. Islam, M. Chakraborty, S. Serniabad, M.S. Khan, D.S. Qais, M.E. Quayum, M.A. Alam, I.M.I. Ismail, M. Tabata, Kinetics and mechanism of incorporation of zinc(II) into tetrakis(1-methylpyridium-4-yl)porphyrin in aqueous solution, Arab. J. Chem. 13 (2020) 6552–6558, https://doi.org/10.1016/j.arabjc.2020.06.011.
[65] F. Wang, X. Qin, D. Zhu, Y. Meng, Li Yang, Y. Ming, PEG-assisted hydrothermal synthesis and photoluminescence of flower-like ZnO microstructures, Mater. Lett. 117 (2014) 131–133, https://doi.org/10.1016/j.matlet.2013.11.108.
[66] Wikipedia. https://en.wikipedia.org/wiki/Proton_affinity.
[67] Z. Li, Y. Xiong, Y. Xie, Selected-control synthesis of ZnO nanowires and nanorods via a PEG-assisted route, Inorg. Chem. 42 (2003) 8105–8109, https://doi.org/10.1021/ic034029q.
[68] H.-M. Xiong, D.G. Shchukin, H. Möhwald, Y. Xu, Y.-Y. Xia, Sonochemical synthesis of highly luminescent zinc oxide nanoparticles doped with magnesium(II), Angew. Chem., Int. Ed. 48 (2009) 2727–2731, https://doi.org/10.1002/anie.200805590.
[69] L. Tang, Y. Cai, G. Yang, Y. Liu, G. Zeng, Y. Zhou, S. Li, J. Wang, S. Zhang, Y. Fang, Y. He, Cobalt nanoparticle-embedded magnetic ordered mesoporous carbon for highly effective adsorption of rhodamine B, App. Surf. Sci. Els. Chem. 314 (2014) 746–753, https://doi.org/10.1016/j.apsusc.2014.07.060.
[70] G. Jethave, U. Fegade, R. Rathod, J. Pawar, Dye pollutants removal from waste water using metal oxide nanoparticle embedded Activated Carbon: an Immobilization study, J. Dis. Sci. Tech. Chem. 40 (2018) 563–573, https://doi.org/10.1080/01932691.2018.1472016.
[71] A. Degen, M. Kosec, Effect of pH and impurities on the surface charge of zinc oxide, J. Eur. Ceram. Soc. 20 (2000) 667–673, https://doi.org/10.1016/S0955-2219(99)00203-4.
[72] I. Langmuir, Adsorption of gases on plane surfaces of glass, mica and platinum, J. Am. Chem. Soc. 40 (1918) 1361–1403, https://doi.org/10.1021/ja02242a004.
[73] H. Freundlich, Adsorption in solutions, J. Phys. Chem. 57 (1906) 384–410.
[74] O. Redlich D.L. Peterson, A useful adsorption isotherm, J. Phys. Chem. 63 (1959) 1024, https://doi.org/10.1021/j150576a611.
[75] M.J. Temkin, V. Pyzhev, Recent modifications to Langmuir isotherms, Acta Physiochim. USSR 12 (1940) 217–222. https://www.sid.ir/En/Journal/ViewPaper.aspx?ID=312965.
[76] E. Abdelkader, L. Nadjia, V. Rose-Noëlle, Adsorption of Congo red azo dye on nanosized SnO_2 derived from sol-gel method, Int. J. Ind. Chem. 7 (2016) 53–57, https://doi.org/10.1007/s40090-015-0061-9.
[77] M. Malakootian, H.J. Mansoorian, A. Hosseini, N. Khanjani, Evaluating the efficacy of alumina/carbon nanotube hybrid adsorbents in removing Azo Reactive Red 198 and Blue 19 dyes from aqueous solutions, Process Saf. Environ. Protect. 96 (2015) 125–137, https://doi.org/10.1016/j.psep.2015.05.002.
[78] F. Salaimi, K. Tahmasobi, C. Karami, A. Jahangiri, Preparation of modified nano-SiO_2 by bismuth and iron as a novel remover of methylene blue from water solution, J. Mex. Chem. Soc. 61 (2017) 250–259, https://doi.org/10.29356/jmcs.v61i3.351.
[79] J. Sun, T. Song, J. Wang, X. Guo, L. Su, W. Tu, Enhanced selective adsorption ability of Cu_2O nanoparticles for anionic dye by sulfur incorporation, SN Appl. Sci. 2 (2020) 1103, https://doi.org/10.1007/s42452-020-2914-x.
[80] A. Yakar, A. Ünlü, T. Yeşilçayır, I. Bıyık, Kinetics and thermodynamics of textile dye removal by adsorption onto iron oxide nanoparticles, Nanotechnol. Environ. Eng. 5 (2020) 6, https://doi.org/10.1007/s41204-020-0068-0.
[81] Z. Wang, P. Yin, R. Qu, H. Chen, C. Wang, S. Ren, Adsorption kinetics, thermodynamics and isotherm of Hg(II) from aqueous solutions using buckwheat hulls from Jiaodong of China, Food Chem. 136 (2013) 1508–1514, https://doi.org/10.1016/j.foodchem.2012.09.090.
[82] Y. Zhang, D. Wang, X. Zhang, F. Qu, Template-free synthesis of porous Cu2O nanospheres at room temperature and investigation on their adsorption property, J. Nanomater. 2013 (2013) 1–5, https://doi.org/10.1155/2013/378919.
[83] C. Duran, D. Ozdes, A. Gundogdu, H.B. Senturk, Kinetics and isotherm analysis of basic dyes adsorption onto Almond shell (Prunus dulcis) as a low-cost adsorbent, J. Chem. Eng. Data 56 (2011) 2136–2147, https://doi.org/10.1021/je101204j.
[84] Y. Li, H. Xiao, M. Chen, Z. Song, Y. Zhao, Absorbents based on maleic anhydride-modified cellulose fibers/diatomite for dye removal, J. Mater. Sci. 49 (2014) 6696–6704, https://doi.org/10.1007/s10853-014-8270-8.
[85] A. Hameed, N. Dewayanto, D. Dongyun, M. Nordin, M. Rahim, Kinetic and thermodynamic of methylene blue adsorption onto zero valent iron supported on mesoporous Silica, Bull. Chem. React. Eng. Catal. 11 (2016) 250–261, https://doi.org/10.9767/bcrec.11.2.443.250-261.
[86] X. Huo, Y. Zhang, J. Zhang, P. Zhou, R. Xie, C. Wei, Y. Liu, N. Wang, Selective adsorption of anionic dyes from aqueous solution by nickel (II) oxide, J. Wa. Sup. Res. Tech. Aqua 68 (2019) 171–186, https://doi.org/10.2166/aqua.2019.115.
[87] G. Mohamed, O.I. Elshafey, N. Fathy, Preparation of carbonaceous hydrochar adsorbents from cellulose and lignin derived from rice straw, Egypt. J. Chem. 60 (2017) 793–804, https://doi.org/10.21608/ejchem.2017.1311.1080.
[88] F. Salaimi, M. Eskandari, C. Karami, Investigation of methylene blue adsorption in wastewater using nano-zeolite modified with copper, Desalination Water Treat. 85 (2017) 206–214, https://doi.org/10.5004/dwt.2017.21248.
[89] Chemical book. Acid blue 92. https://www.chemicalbook.com/ChemicalProductProperty_EN_CB6166546.htm.
[90] D. Balarak, Y. Mahdavi, E. Bazrafshan, A. Mahvi, Kinetic, isotherms and thermodynamic modeling for adsorption of acid blue 92 from aqueous solution by modified Azolla filicoloides, Fresen. Environ. Bul.l 25 (2016) 1321–1330.
[91] A. Goshadrou A, A. Moheb, Continuous fixed bed adsorption of CI Acid Blue 92 by exfoliated graphite: an experimental and modeling study, Desalination 269 (2011) 170–176, https://doi.org/10.1016/j.desal.2010.10.058.
[92] K. Badii, F.D. Ardejani, M.A. Saberi, S. Abdolreza, R.H. Nasab, Adsorption of basic organic colorants from an aqua binary mixture by diatomite, Prog. Color Colorants Coat 5 (2012) 101–116. https://pccc.icrc.ac.ir/article_75765_31f398360da392a86ba5b76e2efda800.pdf.